VOLUME 20 NUMBER 1

ACCOUNTS OF CHEMICAL RESEARCH

JANUARY, 1987

Electron Spin Echo Studies of the Location and Coordination of Metal Species on Oxide Surfaces

LARRY KEVAN

Department of Chemistry, University of Houston, Houston, Texas 77004

Received February 27, 1986 (Revised Manuscript Received September 15, 1986)

Introduction

Paramagnetic metal species are often substituted onto oxide surfaces to generate a catalytic reactive species or site. The structure of this site and the adsorbate geometry is of considerable importance for understanding the chemistry on such surfaces. A sufficiently good understanding of the location and adsorbate structure of catalytically active metal species on oxide surfaces may allow optimization and control of the catalytic activity of such systems. In my laboratory at the University of Houston we have been developing the utilization of a pulsed electron spin resonance (ESR) method known as electron spin echo modulation (ESEM) spectrometry to obtain new geometrical information about such catalytically important surface systems. The ESEM method is particularly well adapted for studying powder spectra in high-surface-area solids. By analyzing the modulation signal which is associated with very weak electron–nuclear dipolar hyperfine interactions it is possible to locate a paramagnetic species with respect to various surface atoms and with respect to adsorbate molecules as well as to determine the number of such nearby atoms or molecules. Ordinary ESR normally does not allow such detailed structural information to be obtained. In this Account we summarize the types of structural conclusions that are being developed about catalytically active metal species on oxide surfaces by utilization of ESR and ESEM spectrometries.

ESEM spectrometry can be illustrated by Figure 1. Spin echoes can be produced in response to suitable resonant microwave pulse sequences in a magnetic resonance experiment. The pulse sequences reorient the magnetic dipoles such that they dephase and rephase while subject to all time-dependent magnetic interactions in the system. The rephasing of the magnetic dipoles to reform macroscopic magnetic moments constitutes the echo. A two-pulse sequence is shown at the top of Figure 1 with the echo denoted by E. As the time between the two pulses (τ) is varied, the echo amplitude traces out a decay envelope which may be modulated as shown in Figure 1 due to weak electron–nuclear hyperfine interactions. Thus, analysis of this modulation affords a way to measure the weak electron–nuclear hyperfine interactions and allows determination of the number and distance of these interacting magnetic nuclei.[1-3]

Both two-pulse and three-pulse echo sequences are used. In the three-pulse sequence shown at the bottom of Figure 1, the second pulse of the two-pulse sequence is essentially divided into two parts. This means that there are two experimentally controllable times in the experiment, τ between the first and second and T between the second and third pulses. It is therefore possible to suppress one nuclear modulation frequency by appropriate selection of one of these times.[1] This allows us to study hyperfine interactions of adsorbate molecules relative to a paramagnetic probe while suppressing hyperfine interactions with the surface framework nuclei. This is particulary important for looking at adsorbate interactions with paramagnetic species on zeolites which contain aluminum as a magnetic surface framework nucleus because aluminum modulation can be suppressed. It is also noteworthy that it is possible to easily see deuterium modulation while suppressing proton modulation when both nuclei are present in the same molecule by selecting the proper pulse amplitude.[1] This occurs because of the significant difference in the nuclear frequency of protons vs. deuterons. This is quite useful because it allows the determination of the *orientation* of an adsorbed molecule with respect to a paramagnetic probe by using selective

Larry Kevan is Cullen Professor of Chemistry at the Unversity of Houston. He was born in Kansas City in 1938 and attended the University of Kansas for his B.S. degree and UCLA for his Ph.D. He was on the faculties of the Univeristy of Chicago, University of Kansas, and Wayne State University before moving to Houston in 1980. He became enthusiastic about the application of electron spin echo spectrometry to chemistry following a voluntary winter in Siberia in 1974 at the Institute of Chemical Kinetics.

(1) Kevan, L. In *Time Domain Electron Spin Resonance*; Kevan, L.; Schwartz, R. N., Eds.; Wiley-Interscience: New York, 1979; pp 279–341.
(2) Ichikawa, T.; Kevan, L.; Bowman, M. K.; Dikanov, S. A.; Tsvetkov, Yu. D. *J. Chem. Phys.* **1979**, *71*, 1167.
(3) Kevan, L. *J. Phys. Chem.* **1981**, *85*, 1628.

0001-4842/87/0120-0001$01.50/0

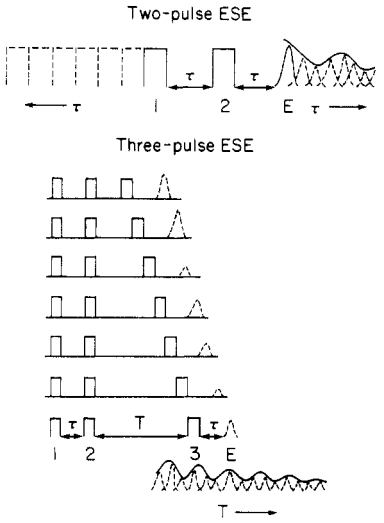

Figure 1. Illustration of modulation of two- and three-pulse electron spin echo decay. In the two-pulse experiment microwave pulses 1 (90°) and 2 (180°) separated by time τ produce the echo signal at time τ after pulse 2. As τ is increased, the echo amplitude changes and traces out an echo envelope which may be modulated. In the three-pulse experiment the second pulse is split into two 90° pulses separated by time T. As T is swept, the echo amplitude changes and traces out an echo envelope which may be modulated.

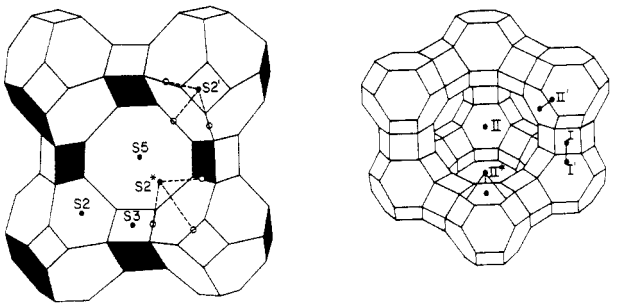

Figure 2. The left side shows a structural model of A zeolite composed of four truncated octahedral sodalite units connected by cubes. Cation site locations are designated S2, S3, etc.; there is no S1 site. The right side shows a structural model of X zeolite composed of sodalite units connected by hexagonal prisms. Cation site locations are designated I, II, etc.

deuteration in different parts of the molecule. An example is methanol adsorbate in which either the hydroxyl group or the methyl group can be deuterated and thus distances to two different positions in the methanol molecule can be measured.

Two types of oxide surfaces are being studied. One is silica or silica gel with the formula SiO_2. The other class of surface materials studied is zeolites[4-6] which are crystalline aluminosilicates. The AlO_4 and SiO_4 tetrahedra are bonded together to form a sodalite or β-cage having eight hexagonal and six square faces. Among the most common zeolites are structural types denoted as A, X, and Y. In A-type zeolites the sodalite units are interconnected by cubes on some of their square faces to form a supercage or α-cage. In X-type zeolites the sodalite units are interconnected by hexagonal prisms on some of their hexagonal faces to form a larger α-cage. Figure 2 shows the A and X zeolite structures.

Because of the presence of aluminum atoms in the zeolite structure, there is a net negative charge in the lattice, and charge compensating cations, typically sodium, are required to balance the anionic framework charge. Other cations are relatively easily exchangeable. The cation locations are crucial to understanding both the catalytic and sorbtive aspects of zeolite surface chemistry. Figure 2 also shows possible cation sites in A and X zeolites.

(4) Rabo, J. A. *Zeolite Chemistry and Catalysis*; American Chemical Society: Washington, DC, 1976.
(5) Breck, D. W. *Zeolite Molecular Sieves*; Wiley-Interscience: New York, 1974.
(6) Barrer, R. M. *Zeolite and Clay Minerals as Sorbents and Molecular Sieves*; Academic Press: New York, 1978.

Table I.
Dominant Cupric Ion Species in A Zeolites[a]

zeolite	hydrated	partially dehydrated	dehydrated	rehydrated
Li_{12}–A, Na_{12}–A	$Cu_{III}(S2^*)$	$\rightarrow Cu_{II}(S2)$	$\rightarrow Cu_0(S2')$	$\rightarrow Cu_{III}(S2^*)$
K_{12}–A	$Cu_I(S2^*)$	$\rightarrow Cu_{II}(S2)$	$\rightarrow Cu_0(S2')$	$\rightarrow Cu_I(S2^*)$
$Tl_{11}Na$–A	$Cu_{III}(S2')$	$\rightarrow$	$Cu_0(S2')$	$\rightarrow Cu_{III}(S2')$
$Rb_{10}Na_2$–A, Cs_7Na_5–A, $(NH_4)_{12}$–A	$Cu_I(S2^*)$	$\rightarrow Cu_{II}(S2)$	$\rightarrow Cu_0(S2')$	$\rightarrow Cu_I(S2^*)$

[a] The Roman numeral subscript gives the number of directly coordinated waters, and the probable zeolite site positions are given in parentheses.

The unit cell formula of four types of zeolites that we have studied in some detail are as follows where the cation has been taken as sodium.

$$\text{A} \quad [Na_{12}(AlO_2)_{12}(SiO_2)_{12}\cdot 27H_2O]_8$$

$$\text{ZK4} \quad [Na_{6-11}(AlO_2)_{6-11}(SiO_2)_{18-13}\cdot yH_2O]_8$$

$$\text{X} \quad Na_{86}(AlO_2)_{86}(SiO_2)_{106}\cdot 264H_2O$$

$$\text{Y} \quad Na_{56}(AlO_2)_{56}(SiO_2)_{136}\cdot 253H_2O$$

Note that A zeolite has a Si/Al ratio of unity. The Si/Al ratio affects the acidity, cation number, and catalytic activity of the zeolite so it is a useful structural parameter to be able to vary. The zeolite termed ZK4 has the A-zeolite strucure with a Si/Al ratio variable between about 1 to 3. Zeolite X has Si/Al $\simeq$ 1.2 and zeolie Y has the X-zeolite structure with Si/Al $\simeq$ 2.4.

The α-cage free-entrance diameter varies with zeolite structure and is ~0.42 nm in *A* zeolite and ~0.74 nm in X zeolite. This gives rise to molecular sieving properties for sorption and for catalysis. The free-entrance diameter to the β-cage is ~0.22 nm. The specific cation present may change the effective entrance diameter to the α- and β-cages by sitting in or near the entrances; this also affects the molecular sieving properties.

We have found that ESEM combined with ESR is a powerful and useful approach for studying paramagnetic cation location and coordination with adsorbates on zeolites and silica. The cupric ion has been studied in the most detail, although other more catalytically important metal ions such as rhodium(II), palladium(I), and palladium(III) are being effectively studied currently. It is of particular significance that a measure of control of the metal ion location and adsorbate coordination has been achieved based on various sample pretreatments.

Cupric Ions in A Zeolites

Cupric ions have proved to be very fruitful probes in zeolites. Of particular interest is the fact that the cupric ion relocates upon partial or complete dehydration of the zeolite. In addition, there is less than one cupric ion per unit cell after exchange of one or two (depending on valence) of the major charge compensating cations

ion the zeolite, and it has been found that the major cation in the zeolite significantly affects the location of the cupric ion probe and its adsorbate interactions.

Table I summarizes the dominant cupric ion locations and water coordination in A zeolites with different major cations as a function of progressive dehydration based on ESR and ESEM data. It should be emphasized that the assignments in Table I have evolved as more experimental studies have been carried out and the sample preparation conditions better controlled; thus these current assignments supersede some previous ones.

In the hydrated A zeolites the size of the major cation plays a controlling role in the water coordination of cupric ion. In Li_{12}–A and Na_{12}–A the cupric ion is coordinated to three waters (Cu_{III}) based on ESEM data, and the ESR parameters are consistent with a distorted octahedral geometry.[7,8] With the larger cations in K_{12}–A and $Tl_{11}Na$–A both Cu_I and Cu_{III} species are observed with similar abundances; one or the other of these species dominates depending on the particular sample preparation. In addition to quite different ESEM spectra consistent wth the different water coordination, Cu_I and Cu_{III} have distinctly different ESR parameters. The parameters for Cu_I are $g_\parallel = 2.479$, $g_\perp = 2.129$, and $A_\parallel = 100 \times 10^{-4}$ cm^{-1}, while the parameters for Cu_{III} are $g_\parallel = 2.345$, $g_\perp = 2.070$, and $A_\parallel = 166 \times 10^{-4}$ cm^{-1}. The parameters of Cu_I are consistent with tetrahedral geometry.[9] With still larger cations in $Rb_{10}Na_2$–A and $(NH_4)_{12}$–A, the Cu_I species is the dominant or only species observed in the hydrated zeolites.

The locations of the Cu_{III} and Cu_I species in hydrated A zeolites have been determined indirectly from dehydration and adsorbate experiments. In all the A zeolites studied, partial dehydration generates a new Cu_{II} species with "reversed" g values ($g_\perp > g_\parallel$) characteristic of a $d_{3z^2-r^2}$ ground state. The most probable geometry to explain the formation of this Cu_{II} species from both Cu_{III} and Cu_I is trigonal bipyramidal coordination in site S2 with three zeolitic oxygens of the 6-ring together with one water in the α-cage and one water in the β-cage. This implies that both Cu_{III} and Cu_I are located in the α-cage at site S2* and that upon partial dehydration both cupric ions move to S2 and pick up coordination with one additional water in the β-cage. In this process Cu_{III} loses two of its waters since water in the larger α-cage is lost more readily than water in the smaller β-cage. Complete dehydration is consistent with Cu^{2+} moving to S2' in the β-cage. This site assignment is supported by subsequent adsorption in Na–A of ethylene which is too large to enter the β-cage. ESEM measurements show that Cu^{2+} interacts weakly with one ethylene at a distance consistent with Cu^{2+} being located about 0.12 nm into the β-cage from the 6-ring window at site S2'.[10]

Although the Cu_{III} species in K–A has similar ESR parameters to those of Cu_{III} in Na–A, the Cu_{III} in K–A has greater stability to dehydration. Upon partial dehydration of K–A Cu_I disappears to largely form Cu_{II} while Cu_{III} remains. This suggests that Cu_{III} formed in initially hydrated K–A is in the β-cage at S2' in contrast to Cu_{III} in Na–A being at S2* in the α-cage. This is consistent with the α-cage cation crowding argument to be discussed next.

Table II.
Interconversion Diagram of Cupric Ion Species in ZK4 Zeolites[a]

K-ZK4 (Si/Al = 1.3)

$Cu_I(S2^*) \xrightarrow{\Delta} Cu_{II}(S2) \xrightarrow{\Delta} Cu_{0'}(S2')$
$\quad\quad \searrow^{\Delta} Cu_{0''}(S2^*)$
$Cu_{III}(S2') \xrightarrow{\Delta} Cu_{0'}(S2')$

K-ZK4 (Si/Al = 1.9)

$Cu_{II'}(S3 \text{ or } S2^*) \xrightarrow{\Delta} Cu_{0''}(S3 \text{ or } S2^*)$
$Cu_{III}(S2') \xrightarrow{\Delta} Cu_{0'}(S2')$
$Cu_I(S2^*) \xrightarrow{\Delta} Cu_{II}(S2) \xrightarrow{\Delta} Cu_{0'}(S2')$

K-ZK4 (Si/Al = 2.4)

$Cu_{II'}(S3 \text{ or } S2^*) \xrightarrow{\Delta} Cu_{0''}, Cu_{0'''}$ (S3 or S2*)
no $Cu_{III}(S2')$ or $Cu_I(S2^*)$ observed; no $Cu_{II}(S2)$ observed on heating

[a] The Roman numeral subscripts give the number of directly coordinated waters and the probable zeolite site positions are given in parentheses. The various Cu_0 primed species differ in their $g_\parallel$ and $A_\parallel$ values.

The main difference between Li^+ and Na^+ vs. K^+, Rb^+, and Cs^+ is in cation size. In addition, X-ray diffraction of Na–A[11] shows that the Na^+ associated with the 6-ring windows is displaced ~0.05 nm into the α-cage whereas K^+ in K–A[12] and Tl^+ in Tl–A are displaced ~0.15 nm into the α-cage. The larger cations projecting further into the α-cage introduce increased electrostatic and steric repulsions in the α-cage leading to α-cage crowding. This is believed to be the reason why Cu_{III} is not formed in the α-cage in A zeolites with larger cations while Cu_I, with reduced steric interactions, is formed.

In addition to changing the size of the major cation in A zeolites to affect α-cage crowding, it is also possible to increase the Si/Al ratio above unity as in normal A zeolites. Such as increase in Si/Al decreases the number of cations required for charge compensation per unit cell. In order to change the Si/Al ratio within the A-zeolite structure, it is necessary to prepare a class of zeolites known as type ZK4 which can be prepared by using the organic template technique in hydrothermal zeolite synthesis.[13] We have studied K–ZK4 zeolites prepared with Si/Al ratios varying from 1.3 to 2.4.[14] The results are summarized in Table II. K–ZK4 (Si/Al = 1.3) has about the same cupric ion species and behavior on dehydration as does K–A except that the Cu_0 species have somewhat different ESR parameters as denoted by the primes on the subscript. This difference could be caused by the asymmetric electrostatic field from a 6-ring when Si/Al $\neq$ 1. In K–ZK4 (Si/Al = 1.9) a new cupric ion species coordinated to two water molecules is observed to dominate instead of Cu_I; this $Cu_{II'}$ species does not have reversed g values so it not assigned to site S2. Instead it is assigned to S3 or S2* and is believed to arise from a decrease in α-cage crowding as the number of K^+ ions decreases in the α-cage consistent with the higher Si/Al ratio. Note that

(7) Kevan, L.; Narayana, M. *ACS Symp. Ser.* **1983**, *218*, 283.
(8) Narayana, M.; Kevan, L. *J. Chem. Soc., Faraday Trans. 1* **1986**, *82*, 213.
(9) Narayana, M.; Kevan, L. *J. Phys. C* **1983**, *16*, 361.
(10) Ichikawa, T.; Kevan, L. *J. Am. Chem. Soc.* **1981**, *103*, 5355.
(11) Yanagida, R. Y.; Amaro, A. A.; Seff, K. *J. Phys. Chem.* **1973**, *77*, 805.
(12) Leung, P. C. W.; Kunz, K. B.; Seff, K.; Maxwell, I. E. *J. Phys. Chem.* **1975**, *79*, 2157.
(13) Jarman, R. H.; Mechoir, M. T.; Vaughn, D. E. W. *ACS Symp. Ser.* **1983**, *218*, 267.
(14) Anderson, M. W.; Kevan, L. *J. Phys. Chem.* **1986**, *90*, 3206.

Table III.
Dominant Cupric Ion Species in X and Y Zeolites[a]

zeolite	hydrated	partially dehydrated	dehydrated	rehydrated
Na–X	$Cu_0(SI)$	$\rightarrow Cu_0(SI)$	$\rightarrow Cu_0('SI')$	$\rightarrow Cu_0(SI)$
Na–Y	$Cu_{III}(SII^*)$	$\rightarrow$	$Cu_0(SI)$ $\rightarrow$	$Cu_0(SI)$
K–X	$Cu_{III}(SII^*)$	$\rightarrow Cu_{II}(SII)$	$\rightarrow Cu_0('SI')$	$\rightarrow Cu_{III}(SII^*)$
K–Y	$Cu_{III}(SII^*)$	$\rightarrow$	$Cu_0(SI)$ $\rightarrow$	$Cu_{III}(SII^*)$
Tl–X	$Cu_{IV}(SV)$	$\rightarrow Cu_{III}(SII^*)$	$\rightarrow Cu_0(SII'$ & $SI)$	$\rightarrow Cu_{VI}(SV)$
Ca–X	$Cu_{II'}(SII)$	$\rightarrow$	$Cu_0(SI')$ $\rightarrow$	$Cu_0(SI')$
	$Cu_{III}(SII^*)$	$\rightarrow$	$Cu_0(SI')$ $\rightarrow$	$Cu_{II'}(SII)$
Cd–X	$Cu_{II'}(SII)$	$\rightarrow$	$Cu_0(SII')$ $\rightarrow$	$Cu_{II}(SII)$
Be–X, Mg–X, Ba–X, Zn–X	$Cu_{III}(SII^*)$			

[a] The Roman numeral subscripts give the number of directly coordinated waters (except II′ refers to two hydroxyls instead of waters), and the probable zeolite site positions are given in parentheses.

partial dehydration does not convert $Cu_{II'}$ to Cu_{II} at S2; instead the Cu_{II} species seems to arise from the smaller amounts of Cu_I. This might suggest that $Cu_{II'}$ is at S3 opposite a 4-ring with distorted square planar coordination to two zeolitic oxygens of the 4-ring and two waters.

Some of the Cu_{III} (S2′) species seen in K–A is also observed in K–ZK4 (Si/Al = 1.3 to 1.9), but it is not seen in K–ZK4 (Si/Al = 2.4). X-ray diffraction results on K–A show that 2 K^+ move into the β-cage on dehydration. Perhaps this may also happen when the Si/Al ratio increases in K–ZK4. This could cause β-cage crowding and prevent the formation of Cu_{III} (S2′).

Thus by varying the cation size and the Si/Al ratio it is possible to achieve two dimensions of control of the cupric ion location and coordination within the A-zeolite-type structure. The reasons for this control are thought to be related to steric and electrostatic factors associated with the number and position of the cations in the α- and β-cages.

Cupric Ions in X and Y Zeolites

Cupric ion location and coordination in X and Y type zeolites are summarized in Table III. Refer to Figure 2 for the cation sites in X or Y zeolites. In X zeolites a strong effect is again found due to the nature of the major cation present. The cupric ion location and coordination can be changed by converting Na–X to K–X zeolite.[15] In Na–X zeolite the cupric ion is initially located in site SI in the hexagonal prism of the X zeolite structure and is not directly coordinated to any water molecules because there is not sufficient room for directly coordinated water molecules within the hexagonal prism. As water is removed from the sodium X zeolite by thermal dehydration, the cupric ion remains in the hexagonal prism. However if Na^+ is replaced by K^+ the cupric ion is initially found to be located in the α-cage at site SII* coordinated to three water molecules. As thermal dehydration proceeds a Cu_{II} species with reversed g values ($g_\perp > g_\parallel$) characteristic of trigonal bipyramidal coordination at site SII can be detected. Finally after complete dehydration the cupric ion moves into the hexagonal prism which is the same final site in dehydrated K–X as in Na–X. Arguments for the different initial location of cupric ion in hydrated Na–X and K–X zeolites have been advanced on the basis of the greater hydration energy of Na^+ vs. K^+ so that the cupric ion initially displaces Na^+ from the hexagonal prism site whereas the energy for this to occur with K^+ is not quite sufficient.[15]

A difference between X- and Y-type zeolites is also found.[16] Recall that the Y zeolites have a larger Si/Al ratio and hence have a lower Coulomb energy at SI in the hexagonal prism. Thus one finds that cupric ion in Na–Y zeolite is initially located in the α-cage at SII* coordinated to three water molecules. This is the same site as found in K–X zeolite. As thermal dehydration proceeds the cupric ion moves through site SII into the hexagonal prism site as expected. The behavior of cupric ion in K–Y zeolite is identical with that for Na–Y zeolite. However after full dehydration, rehydration of Na–Y zeolite shows a different behavior from rehydration of K–Y zeolite. In Na–Y rehydration does not move the cupric ion from its hexagonal prism site as is also found for Na–X zeolite. Thus a rehydrated Na–Y zeolite has a different cupric ion location and coordination than an initially hydrated Na–Y zeolite. This must be due to the delicate balance of the hydration energies of the alkali metal cations within the Y-zeolite structure.

In contrast, K–Y rehydration causes the cupric ion to move from the hexagonal prism site back to the α-cage site coordinated to three water molecules which is identical with the initially hydrated situation in K–Y zeolites. In K–X rehydration also moves the cupric ion from the hexagonal prism site to the α-cage coordinated to three waters which again is identical with the initially hydrated state of K–X zeolite.

Thus in all the X and Y dehydrated zeolites that have been described the cupric ion always ends up in the hexagonal prism site whereas in hydrated or rehydrated X and Y zeolites it is possible to control whether the cupric ion remains in the hexagonal prism site or moves out to the α-cage coordinated to several water molecules by selecting X vs. Y zeolite and sodium vs. potassium ion substitution.

The effect of other major cations in X zeolites has also been investigated to some extent. Tl–X zeolite is particularly interesting in that the initially hydrated form shows cupric ion coordinated to six waters which is the same as in bulk aqueous solution and located in the middle of the α-cage at site SV.[17,18] Partial dehydration will convert this to the cupric ion located at site SII* coordinated to three waters as seen in sodium and potassium X zeolites and complete dehydration moves the cupric ion toward the hexagonal prism. However in the completely dehydrated Tl–X zeolite there appear to be two cupric ion species present. Rehydration regenerates the cupric ion coordinated to six waters in the middle of the α-cage.

For divalent major cations in X zeolites such as Be–X, Mg–X, Ba–X, and Zn–X, the major cupric species seen in the hydrated zeolites is Cu_{III} located in the α-cage in site SII*. However Ca–X[20] and Cd–X[21] only show a trace of this Cu_{III} species and show predominantly a cupric ion located in the six-ring site SII coordinated to two adsorbate species in a trigonal bipyramidal structure. These adsorbate species are suggested to be

(15) Ichikawa, T.; Kevan, L. *J. Am. Chem. Soc.* **1983**, *105*, 402.
(16) Ichikawa, T.; Kevan, L. *J. Phys. Chem.* **1983**, *87*, 4433.
(17) Narayana, M.; Kevan, L. *Proceedings of the Sixth International Zeolite Conference*, Butterworth Scientific: London, 1984, p 774.
(18) Lee, H.; Narayana, M.; Kevan, L. *J. Phys. Chem.* **1985**, *89*, 2419.
(19) Narayana, M.; Kevan, L., unpublished results.
(20) Narayana, M.; Kevan, L. *J. Chem. Phys.* **1983**, *78*, 3573.
(21) Narayana, M.; Kevan, L. *Langmuir* **1986**, *1*, 553.

hydroxyl groups based on thermal stability arguments.

So in the X-type zeolites as in the A-type zeolites it is found that a degree of control of the cupric ion location can be achieved by varying the major cation present as well as the Si/Al ratio and the thermal pretreatment.

Rhodium Species in X Zeolites

A series of recent studies focuses on paramagnetic rhodium species in X zeolites.[22-24] Rhodium(III) is exchanged into Na–X zeolite via a rhodium pentaamine chloride complex to an extent of less than one rhodium ion per unit cell. By heating this exchanged zeolite in flowing oxygen at varying temperatures different paramagnetic Rh(II) species can be formed. The two major species are denoted as Rh^{2+}(A) generated as a predominant species at an activation temperature of around 320 °C and Rh^{2+}(C) generated as a major species around 450 °C. By analyzing associated ESEM spectra and looking at broadening effects on the ESR spectrum by the introduction of oxygen it is concluded that the Rh^{2+}(A) species is located in the β-cage at site SII′ and is not directly coordinated to water. However, addition of adsorbate water to this species converts it to the Rh^{2+}(C) species located in the hexagonal prism in site SI where it is weakly coordinated to four water molecules in the β-cage at a rhodium to proton distance of 0.42 nm. If this species is exposed to additional water for a lengthy period of time the Rh^{2+} species appears to be pulled out of the hexagonal prism into the β-cage where it becomes more directly coordinated with two molecules of water with a rhodium to proton distance of 0.30 nm. Another interesting feature of the generation of the paramagnetic rhodium species in the X zeolite is that at an activation temperature of about 410 °C the total spin concentration is very low. This has been explained by the formation of the dimeric Rh(II) species which are diamagnetic and which can be split to form paramagnetic species both by increased temperature and by the addition of different adsorbates such as water, methanol, ethanol, and ammonia.

Reduction by H_2 and oxidation by O_2 of Rh exchanged Na–X has also been studied in some detail by ESR and ESEM.[23] Reduction generates a dominant, a new Rh(II) species in samples activated at 240–400 °C which is suggested to be complexed with H_2 and located in the α-cage. A second species is produced by H_2 redution of samples activated at 400–500 °C, and it seems to be located in the β-cage or hexagonal prism. Thus controlled reduction offers a way to control the location of Rh(II) species.

It has been recently found that the major cation, Na^+ or Ca^{2+}, can affect the Rh(II) species generated in X zeolites and its location.[24] This finding again points to potential control of reactions catalyzed by metal-containing zeolites.

Palladium Species in X Zeolites

Paramagnetic palladium species have also proved interesting and significant to study in X zeolites and a certain measure of control of their location has also been achieved.[25,26] To prepare paramagnetic palladium species in X zeolite the tetraamine complex of Pd(II) is exchanged into the zeolite to an extent of less than one per unit cell which is then heated under vacuum at about 773 K. In Ca–X this produces Pd^0 clusters which show no ESR signal; the reduction apparently occurs by ammonia from the amine complex. Subsequent activation at 773 K in oxygen leads to an isotropic ESR spectrum at $g = 2.23$. This can be assigned to Pd(III) from the nature of its ESR spectrum with further conformation from X-ray photoelectron spectra of similarly prepared samples.[27] It is quite interesting that subsequent evacuation at 773 K causes a significant decrease in this isotropic ESR spectrum and generates a second paramagnetic species characterized by axial g-anisotropy with $g_\perp > g_\parallel \sim 2.10$. This axially symmetric species is assigned to Pd(I) again based on the characteristic of its ESR spectrum with further conformation from X-ray photoelectron spectroscopy.[27] The spectrum obtained after this total activation process of heating under vacuum followed by heating in oxygen followed by heating again under vacuum is shown in Figure 3a. In the final prolonged evacuation at high temperature it is assumed that Pd(0) species migrate in the zeolite and disproportionate with Pd(II)

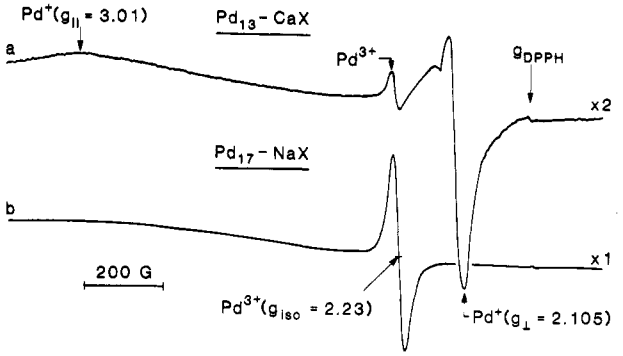

Figure 3. ESR spectra of activated Pd_{13}–CaX (a) and Pd_{17}–NaX (b) zeolites at 77 K.

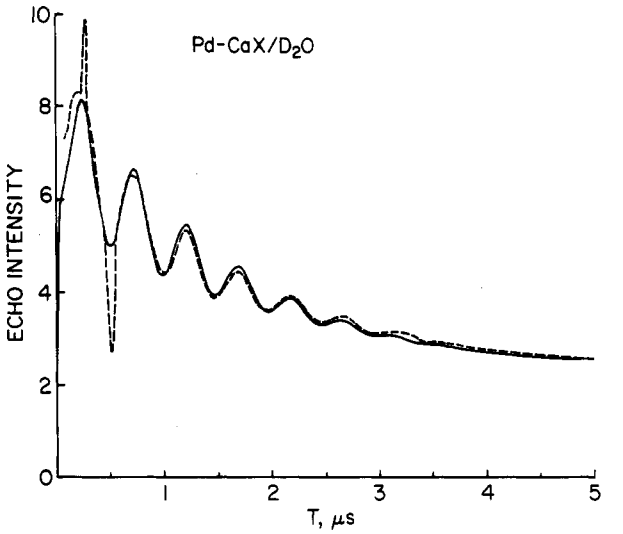

Figure 4. Experimental (dashed) and calculated (solid) three-pulse ESEM spectra of activated Pd–CaX with subsequent hydrogen reduction and D_2O adsorption. The fit corresponds to 4 deuterons at 0.37 nm. The sharp peaks in the dashed curve at ~0.3 and ~0.5 μs are two-pulse interferences.

(22) Goldfarb, D.; Kevan, L. *J. Phys. Chem.* **1986**, *90*, 264.
(23) Goldfarb, D.; Kevan, L. *J. Phys. Chem.* **1986**, *90*, 2137.
(24) Goldfarb, D.; Kevan, L. *J. Phys. Chem.* **1986**, *90*, 5787.
(25) Michalik, J.; Narayana, M.; Kevan, L. *J. Phys. Chem.* **1985**, *89*, 4553.
(26) Michalik, J.; Heming, M.; Kevan, L. *J. Phys. Chem.* **1986**, *90*, 2132.
(27) Narayana, M.; Michalik, J.; Contarini, S.; Kevan, L. *J. Phys. Chem.* **1985**, *89*, 3895.

to form Pd(I) and with Pd(III) to decrease Pd(III).

The location of these palladium species was deduced by experiments with various adsorbates such as water, methanol, ammonia, ethanol, ethylene, and benzene to determine the accessibility of the palladium species to adsorbates of different sizes and ESEM experiments to determine their coordination to various adsorbed molecules. It is found that Pd(III) is in a more accessible site in Ca–X zeolite since it readily reacts with both water and methanol to disappear. In the reaction with water a new paramagnetic species is observed which is identified as a Pd(II)–O_2^- complex in which the water has actually been split by reaction with Pd(III). This suggests that the Pd(III) species is located in the region of a six-ring site probably somewhat displaced into the β-cage since that is where most of the Ca^{2+} ions have been located by X-ray diffraction in Ca–X zeolite.

In contrast, Pd(I) in Ca–X zeolite does not react with water or methanol adsorbates and Figure 4 shows the three-pulse ESEM spectrum of Pd(I) after adsorption of D_2O. The analysis indicates that the Pd(I) interacts with four deuterons or two water molecules but the distance of interaction is long enough, 0.37 nm, that these waters are not directly coordinated. This and other experiments indicate that the Pd(I) species is located in a hexagonal prism site at SI or perhaps displaced slightly into a β-cage at site SI′.

As in the case of the cupric ion studies, it has also been found that there is a strong effect of the major cation in the X zeolite on the location of the paramagnetic palladium species generated by the activation process.[26] This is shown dramatically by the comparison of the ESR spectra generated for the same type of activation process of palladium doped Ca–X and Na–X zeolites in Figure 3. It can be seen that in Na–X zeolite only Pd(III) is generated after the total activation process and that it is not converted in large part to Pd(I) as it is in Ca–X zeolite. This indicates that Pd(III) is more stable in Na–X than in Ca–X zeolite. This also suggests that the location of the Pd(III) in the two zeolites is probably different. The ESEM spectra of Pd(III) in Na–X with adsorbed D_2O show that Pd(III) is most likely in a hexagonal prism site since only indirect coordination with one molecule of D_2O is indicated. Furthermore, no deuterium modulation is observed for adsorbed deuterated benzene or methanol both of which molecules are too big to enter the β-cage.

Although no Pd(I) is indicated in the spectrum in Figure 3b, this paramagnetic state of palladium can be generated in Na–X zeolite by prolonged exposure of Pd(III) to benzene or methanol. The process takes several days at room temperature, but eventually the Pd(III) is partially converted to Pd(I) by a mechanism that is unclear. The Pd(I) that is so formed seems to be located in the β-cage, perhaps close to a six-ring site near SII′ based on more direct coordination of methanol than for Pd(III). Another indication of the difference in location within the zeolite structure of Pd(III) and Pd(I) is shown by aluminum ESEM. The aluminum modulation is much more prominent for the Pd(III) species which is consistent with it being located in a hexagonal prism site with more surrounding aluminums than in a six-ring site such as SII or SII′ which is assigned to Pd(I).

Thus by using either Ca–X or Na–X zeolite it is possible to control the location of either paramagnetic charge state of palladium to be in either a hexagonal prism or in a β-cage site near a six-ring.

Cupric Ions on Silica

Paramagnetic metal species on other oxide surfaces have also been studied to some extent. The most comprehensive studies have been carried out with cupric ion on silica surfaces.[28–31] Here the main focus is to determine differences in adsorbate geometry as the size and polarity of the adsorbate is changed. Not enough is known about the details of the surface structure of silica to locate cupric ion in different specifically distinguishable sites as is possible in zeolites. However a certain degree of control of the coordination geometry can be achieved by different methods of preparation of cupric ion on silica.

The two types of preparation procedures that have been used involve ion exchange[28,29] and impregnation.[30,31] Both techniques are used to prepare metal ions on silica and other oxide surfaces for catalytic purposes. In the ion-exchange process cupric ion is complexed with ammonia and then exchanged for protons in hydroxyl groups on the silica surface. The ammonia ligands can be driven off by thermal means to generate a firmly bound cupric ion. The procedure of impregnation is simply to slurry the silica in a copper salt solution, wash with water, and dry which incorporates more loosely bound cupric ions on the silica surface. The local geometry around cupric ion put on silica in these two ways is not known in detail, but differences can be deduced from subsequently determined adsorbate geometry.

The number of coordinated adsorbate molecules and the distance to them is determined by ESEM spectrometry. In addition some constraints on the probable symmetry is indicated by the relative magnitude of the parallel component of the copper hyperfine interaction ($A_\parallel$) based on studies on specific known cupric compounds. In general, $A_\parallel$ decreases as the geometry changes from square planar to octahedral to tetrahedral. For ion-exchanged cupric ion[29] two molecules of ammonia or pyridine adsorbates are found to be strongly bound. No nitrogen hyperfine interaction is observed in the ESR spectrum, and the geometry is deduced to be approximately square planar with coordination of cupric ion to two adsorbate nitrogens and to two oxygens of the silica surface. For water and methanol the coordination is still quite strong, and two molecules are also indicated as coordinated to the cupric ion, but a smaller $A_\parallel$ value suggests distorted octahedral geometry. By use of specific deuteration the orientation of the methanol molecule with respect to cupric ion can be determined so that the copper–oxygen distance of 0.21 nm can be determined with some degree of confidence. Acetone also coordinates in the same way as methanol with two molecules bound to cupric ion in a distorted octahedral geometry. Only one molecule of ethylene is very weakly bound as indicated by a relatively long interaction distance. The $A_\parallel$ is unresolved which is consistent with distorted tetrahedral geometry. The interaction is so weak that the adsorbate is not in the first coordination shell and a distorted tetrahedral ge-

(28) Ichikawa, T.; Yoshida, H.; Kevan, L. *J. Chem. Phys.* **1981**, *75*, 2485.
(29) Ichikawa, T.; Yoshida, H.; Kevan, L. *J. Phys. Chem.* **1982**, *86*, 881.
(30) Narayana, M.; Zhan, R. Y.; Kevan, L. *J. Phys. Chem.* **1984**, *88*, 3990.
(31) Zhan, R. Y.; Narayana, M.; Kevan, L. *J. Phys. Chem.* **1985**, *89*, 831.

ometry is determined by interaction of cupric ion with four oxygens of the silica surface.

Similar studies on impregnated cupric ion on silica show some general differences in the adsorbate geometries between these two preparation techniques.[30,31] For ion-exchanged cupric ion intense well-resolved ESR spectra are observed whereas for impregnated cupric ion much weaker, more poorly resolved ESR spectra are observed. This is consistent with ion-exchanged cupric ion being more strongly bound to silica than impregnated cupric ion. This implies that the impregnated cupric ion should be more accessible to adsorbates and experiment supports this. The strong binding of ion-exchanged cupric ion on silica seems to prevent cupric ion dimer formation for large concentrations of cupric ion whereas in impregnated samples cupric ion dimer formation or clusters are more readily seen. Adsorbates on impregnated cupric ion on silica do seem to be more strongly bound in general. Ammonia and pyridine again coordinate two molecules to impregnated cupric ion but stronger binding is indicated by the observation of nitrogen hyperfine by ESR. Water and methanol are strongly bound with two coordinated molecules as with ion-exchanged cupric ion. However, for impregnated cupric ion, adsorbed acetone reacts, and no geometrical information can be obtained. Ethylene and CO interact more strongly with impregnated cupric ion than with ion-exchanged cupric ion. This is shown directly for ethylene by ESEM experiments in which the cupric ion to proton distance is 0.41 nm for ion-exchanged cupric ion but only 0.33 nm for impregnated cupric ion on silica. The geometry differs also. For ion-exchanged cupric ion a very weak interaction with a distorted tetrahedral geometry is suggested whereas for impregnated cupric ion a distorted trigonal bipyramidal structure is suggested. This latter geometry is supported by reversed values in the ESR spectrum ($g_\perp > g_\parallel$).

In addition to cupric ion on silica, recent work has focused on ESEM studies of adsorbate geometry of V(IV)[32,33] and Mo(V)[34,35] paramagnetic species on silica.

(32) Narayana, M.; Narasimhan, C. S.; Kevan, L. *J. Catal.* **1983**, *79*, 237.
(33) Narayana, M.; Narasimhan, C. S.; Kevan, L. *J. Chem. Soc., Faraday Trans. 1* **1985**, *81*, 137.

Conclusions

In general we have found that ESEM spectrometry combined with ESR is a useful technique to study the geometry and adsorbate interactions in powders. It has been particularly effective for looking at paramagnetic metal species in zeolites and on silica surfaces. The locations of paramagnetic metal species in both A- and X-type zeolites has been found to be controllable by (a) varying the major cation in the zeolite structure, (b) varying the state of hydration by thermal treatment, (c) changing the type of adsorbate, (d) varying the structural type of the zeolite, and (e) varying the silicon to aluminum ratio in the zeolite structure.

On silica surfaces where the locations of paramagnetic metal ions cannot be assigned to specific sites, it is found that adsorbate coordination and geometry can be determined. It is found that the geometry can be controlled to some extent by incorporating a paramagnetic ion on the silica surface by ion exchange or impregnation.

Current work is oriented toward relating information about the metal species location and adsorbate geometry to the efficiency of specific catalytic reactions. Initial information has been obtained on ethylene dimerization by palladium ions in X zeolites[36] and on propylene oxidation by cupric ions in X- and A-type zeolites.[37,38] More detailed studies of this type should lead to improved understanding of surface catalysis by metal species in terms of the geometrical and structural factors that are of importance.

This work has been generously supported by the National Science Foundation, the Robert A. Welch Foundation, and the Texas Advanced Technology Research Program. I particularly wish to thank a number of excellent coworkers who have made this work possible over the last several years: T. Ichikawa, M. Narayana, H. Lee, R. Y. Zhan, J. Michalik, D. Goldfarb, and M. Anderson.

(34) Narayana, M.; Zhan, R. Y.; Kevan, L. *J. Phys. Chem.* **1985**, *89*, 636.
(35) Zhan, R. Y.; Narayana, M.; Kevan, L. *J. Chem. Soc., Faraday Trans. 1* **1985**, *81*, 2083.
(36) Plonka, A.; Kevan, L. *J. Phys. Chem.* **1985**, *89*, 2087.
(37) Lee, H.; Kevan, L. *J. Phys. Chem.* **1986**, *90*, 5781.
(38) Lee, H.; Kevan, L. *J. Phys. Chem.* **1986**, *90*, 5776.